Mathematical Biosciences 394 (2026) 109645

Contents lists available at ScienceDirect

Mathematical Biosciences

journal homepage: www.elsevier.com/locate/mbs

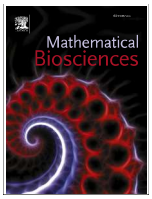

A reduced model for the long-term effects of physical activity on type 2 diabetes

Lea Multerer [a,*], Pierluigi Francesco De Paola [b,c,d], Marta Lenatti [b], Alessia Paglialonga [b], Laura Azzimonti [a]

[a] SUPSI, Dalle Molle Institute for Artificial Intelligence (IDSIA), Lugano, Switzerland
[b] CNR, CNR-IEIIT, Milan, Italy
[c] CNR, CNR-IASI, Rome, Italy
[d] Politecnico of Bari, Bari, Italy

ARTICLE INFO

Keywords:
Reduced model
Ordinary differential equations
Homogenization
Physical activity
Type 2 diabetes
Long-term progression
Computational efficiency

ABSTRACT

Type 2 diabetes progresses slowly and may be reversed through lifestyle changes, but quantifying the long-term impact of regular physical activity remains challenging due to sparse longitudinal data. Mechanistic models offer a powerful tool by simulating metabolic processes over extended timescales. However, multi-scale formulations that capture both the short-term effects of exercise sessions and the slow evolution of disease tend to be computationally demanding, limiting their practical use in personalized decision support.

To address this limitation, we derived a reduced version of a two-scale model that captures the short- and long-term effects of physical activity on blood glucose regulation. By analytically averaging the short-term effects induced by exercise, we developed a homogenized formulation that transmits the average contribution of physical activity to the slower glucose-insulin dynamics. This reduction preserves the key model dynamics while decreasing computational complexity by almost a factor 2000. We prove that the approximation error remains bounded and confirm the model's accuracy through a parameter-based simulation study.

The resulting model provides a mathematically grounded reduction that retains key physiological mechanisms while enabling fast long-term simulations. This substantial computational gain makes it suitable for integration into medical decision support systems, where it can be used to design and evaluate personalized physical activity plans aimed at reducing the risk of type 2 diabetes.

1. Introduction

The progression to type 2 diabetes is asymptomatic, develops over years, and may often be reversed with adequate lifestyle changes [1,2]. Personalized recommendations on modifiable risk factors, such as physical activity, are crucial for preventing or delaying the disease progression [3]. However, longitudinal data capturing the regular impact of physical activity over many years remain scarce, making data-driven assessment of long-term effects infeasible in practice. Mechanistic models offer a way to bridge this gap by simulating the complex physiological mechanisms over long timescales.

Ordinary differential equation models (ODEs) have been widely used to model glucose-insulin interactions, capturing effects ranging from a minute-scale [4,5] to long-term dynamics spanning years or even decades [6–9]. Early minimal models focused on short-term glucose and insulin interactions, using a few state variables [4,10]. Extensions expanded these approaches to include the short-term effects of physical activity [5]. Building on these foundations, a growing range of models captures complex metabolic and inflammatory processes across multiple time-scales [11–13]. Models for long-term disease progression integrate beta-cell dynamics that account for the long-term interactions between glucose and insulin [6]. Subsequent extensions introduce additional state variables to better capture the progression over several years or even decades [7,14,15]. However, these long-term progression models do not incorporate the effects of physical activity on the glucose-insulin dynamics.

Recently, this gap was filled by a model capturing the short- and long-term effects of regular physical activity on blood glucose regulation in terms of twelve ODEs on two timescales [8,9]. This model allows for a mechanistic description of how long-term physiological processes are influenced by the integral effects of physical activity. The model is able to estimate the long-term benefits of physical activity in a variety of

* Corresponding author.
E-mail addresses: lea.multerer@supsi.ch (L. Multerer), p.depaola@phd.poliba.it (P.F. De Paola), martalenatti@cnr.it (M. Lenatti), alessia.paglialonga@cnr.it (A. Paglialonga), laura.azzimonti@supsi.ch (L. Azzimonti).

https://doi.org/10.1016/j.mbs.2026.109645
Received 2 December 2025; Received in revised form 30 January 2026; Accepted 5 February 2026
Available online 9 February 2026

conditions and includes inter-individual variability, for example in terms of response to exercise, exercise program structure and adherence rates, and individual level of risk [9]. As such, the model may be the basis for deriving personalized physical activity recommendations to prevent the progression to type 2 diabetes. However, due to its multi-scale nature, repeated simulations remain computationally intensive, limiting its practical use in decision-support. This calls for a model reduction that preserves the mechanistic grounding while enabling fast, scalable simulation to support clinical decision-making.

A powerful approach to reducing the complexity of multi-scale differential equation models is homogenization [16–20]. It applies to systems with dynamics across multiple scales, such as high-frequency oscillations over time or distinct spatial patterns. The goal is to replace the short-scale oscillations with a smoothed or averaged solution to yield an effective, simplified model that captures the macroscopic dynamics. Common applications include material science [21] and fluid dynamics [22]. Although traditionally used for partial differential equations, homogenization techniques can also be effectively applied to ODEs [23].

In this work, we derive a reduced version of a model that examines the long-term effects of physical activity on blood glucose regulation [8,9], applying principles from homogenization theory to obtain a system of seven ODEs (reduced from twelve). This reduced model preserves the essential long-term influence of physical activity on type 2 diabetes progression while being computationally efficient. We prove the boundedness of the approximation error and inspect it in a numerical simulation study. Our approach leads to a fast approximation of the full model, enabling the efficient prediction of type 2 diabetes progression as a function of physical activity and facilitating personalized physical activity plans for risk reduction. To the best of our knowledge, this is the first application of homogenization theory to mechanistic models of type 2 diabetes progression, linking model reduction with clinically relevant long-term simulations.

The remainder of this paper is structured as follows: In Section 2, we present a scaled version of the full model to improve numerical stability and establish the existence and uniqueness of solutions. Section 3 details the reduction of the short-term state variables and provides a proof of error bounds. In Section 4, we present a numerical comparison of the original and reduced models across various parameters and initial conditions. Finally, Section 5 discusses the implications and contributions of this work.

2. A scaled model for the effect of regular physical activity on type 2 diabetes progression

The system of ODEs under investigation operates on two timescales. The short-term equations describe how the glucose-insulin regulation mechanism is influenced during a physical activity session on a minute-scale. These dynamics exhibit a periodic pattern, repeating with every physical activity session. The long-term equations describe the evolution of glucose regulation over years, parametrized at a day-scale. These dynamics are modulated by physical activity through a coupling with the short-term system.

2.1. Model formulation

We present a scaled, coupled version of the original model formulation for improved numerical stability [24]. The detailed technical steps to transform the original system into the scaled version managing the multiple scales are provided in Appendix A.

We consider the system of ODEs

$$\frac{\mathrm{d}}{\mathrm{d}t}\mathbf{y}(t,u) := \frac{\mathrm{d}}{\mathrm{d}t}\begin{bmatrix}\mathbf{y_1}(t,u)\\ \mathbf{y_2}(t,\mathbf{y_1})\end{bmatrix} = \begin{bmatrix}\mathbf{f_1}(t,u,\mathbf{y_1})\\ \mathbf{f_2}(t,\mathbf{y_1},\mathbf{y_2})\end{bmatrix} =: \mathbf{f}(t,u,\mathbf{y}) \tag{1}$$

for $0 < t \le t_{\text{end}}$, together with the initial condition $\mathbf{y}(0) = \mathbf{y_0}$. The control $u(t)$ is a periodic continuation of a Heaviside function, defined for $n \in \mathbb{N}$ periods as

$$u(t) := \begin{cases} 1 & \text{for } kv \le t \le kv + \delta, \\ 0 & \text{for } kv + \delta < t < (k+1)v, \end{cases} \tag{2}$$

where $k = 0, \dots, n-1$ and $t_{\text{end}} := nv$. The parameter v denotes the period length of physical activity and refers to the time between the start of two consecutive sessions, and δ is the duration of a physical activity session. The vector $\mathbf{y_1}$ contains the short-term equations and comprises 5 state variables

$$\mathbf{y_1} := [VO_2, G_{\text{pr}}, G_{\text{up}}, I_{\text{e}}, IL6]^T,$$

that satisfy the following ODEs

$$\frac{\mathrm{d}}{\mathrm{d}t}\mathbf{y_1} := \frac{\mathrm{d}}{\mathrm{d}t}\begin{bmatrix}VO_2\\ G_{\text{pr}}\\ G_{\text{up}}\\ I_{\text{e}}\\ IL6\end{bmatrix} = \begin{bmatrix}\lambda_t\theta(u(t) - VO_2)\\ \lambda_t\alpha_2(VO_2 - G_{\text{pr}})\\ \lambda_t\alpha_4(VO_2 - G_{\text{up}})\\ \lambda_t\alpha_6(VO_2 - I_{\text{e}})\\ \lambda_t\kappa_{\text{IL6}}(VO_2 - IL6)\end{bmatrix} =: \mathbf{f_1}(t,u,\mathbf{y_1}), \tag{3}$$

together with the initial conditions $\mathbf{y_1}(0) = [0,0,0,0,0]^T$. Details on the constant scaling parameter λ_t and the other parameters θ, α_2, α_4, α_6 and κ_{IL6} are given in Appendix B. The short-term variables $[VO_2, G_{\text{pr}}, G_{\text{up}}, I_{\text{e}}, IL6]^T$ capture the immediate physiological responses to physical activity. Specifically, oxygen consumption (VO_2) drives the other variables during exercise. The rate of increase in hepatic glucose production (G_{pr}) and glucose uptake by working tissues (G_{up}) reflect the acute demand for glucose during activity. The rate of increase in insulin removal from circulation (I_{e}) is enhanced by exercise, while the rate of release of Interleukin-6 ($IL6$), classically pro-inflammatory but functioning as an anti-inflammatory myokine during exercise [25], accounts for its anti-inflammatory effects. These short-term equations are parametrized such that the numerical solution of $\mathbf{y_1}$ increases as soon as physical activity starts and decays fast once it stops again. This yields a periodic pattern of the solution $\mathbf{y_1}$ with period v, with all components remaining bounded within a fixed range for all $t \in [0, t_{\text{end}}]$.

The vector $\mathbf{y_2}$ summarizes the long-term equations and comprises 7 state variables,

$$\mathbf{y_2} := [VL, S_{\text{I}}, \Sigma, \Gamma, B, I, G]^T,$$

that satisfy the following ODEs

$$\frac{\mathrm{d}}{\mathrm{d}t}\mathbf{y_2} := \frac{\mathrm{d}}{\mathrm{d}t}\begin{bmatrix}VL\\ S_{\text{I}}\\ \Gamma\\ \Sigma\\ B\\ I\\ G\end{bmatrix} = \begin{bmatrix}h_{VL}(VL, IL6)\\ h_{S_{\text{I}}}(S_{\text{I}}, VL)\\ h_{\Gamma}(\Gamma, G)\\ h_{\Sigma}(\Sigma, \Gamma, G)\\ h_B(B, VL, \Gamma, \Sigma, G)\\ h_I(I, I_{\text{e}}, \Gamma, \Sigma, B, G)\\ h_G(G, G_{\text{up}}, G_{\text{pr}}, S_{\text{I}}, I)\end{bmatrix} =: \mathbf{f_2}(t, \mathbf{y_1}, \mathbf{y_2}), \tag{4}$$

together with the scaled initial conditions

$$\mathbf{y_2}(0) = [0, 1, \Gamma_{0\lambda}, \Sigma_{0\lambda}, 1, 1, 1]^T.$$

The right hand side functions are defined as follows:

$$h_{VL}(VL, IL6) := \lambda_t\kappa_s(IL6 - VL),$$

$$h_{S_{\text{I}}}(S_{\text{I}}, VL) := d_\lambda(VL)\frac{\theta_{S_{\text{I}}} - \lambda_{S_{\text{I}}}S_{\text{I}}}{\tau_{S_{\text{I}}}},$$

$$h_{\Gamma}(\Gamma, G) := \frac{g_\lambda(G) - \Gamma}{\tau_\Gamma},$$

$$h_{\Sigma}(\Sigma, \Gamma, G) := \frac{s_\lambda(\Gamma, \Sigma, G) - \Sigma}{\tau_\Sigma},$$

$$h_B(B, VL, \Gamma, \Sigma, G) := \frac{p_\lambda(VL, \Gamma, \Sigma, G) - a_\lambda(VL, G)}{\tau_B}B,$$

$$h_I(I, I_{\text{e}}, \Gamma, \Sigma, B, G) := r_\lambda(\Gamma, \Sigma, G)B - \kappa I - \lambda_{I_{\text{e}}I}I_{\text{e}},$$

$$h_G(G, G_{\text{up}}, G_{\text{pr}}, S_{\text{I}}, I) := \rho_\lambda + \lambda_{tG}\omega(\lambda_{G_{\text{pr}}}G_{\text{pr}} - \lambda_{G_{\text{up}}}G_{\text{up}}) - (\eta_0 + \lambda_{S_{\text{I}}I}S_{\text{I}}I)G.$$

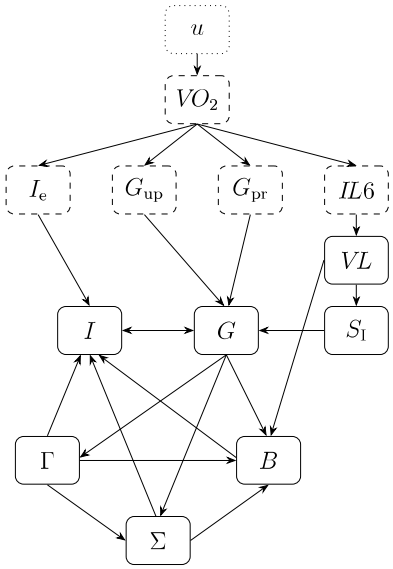

Fig. 1. Structure of the full model $\mathbf{y}(t,u)$. The control u (dotted) influences the short-term state variables grouped together in $\mathbf{y_1}(t,u)$ (dashed) which, in turn, influence the long-term state variables grouped together in $\mathbf{y_2}(t,\mathbf{y_1})$ (solid).

These functions include six auxiliary functions d_λ, g_λ, s_λ, p_λ, a_λ and r_λ that are written out in detail in Eq. (A.1) in Appendix A. These auxiliary functions are compositions of Hill-type functions and fractions incorporating exponential functions. Again, a list of all the parameters introduced are listed in Appendix B.

The long-term equations capture the behavior of glucose regulation over a time span of years. Due to the feedback structure of the system and the boundedness of the short-term variables $\mathbf{y_1}(t)$, these state variables remain bounded over time for the selected set of parameters. The core of this subset of equations lies in the variables $[VL, B, I, G]^T$, modeling the glucose-insulin (G and I) negative feedback loop. This feedback mechanism involves the action of beta cells (B), responsible for insulin release. The variable VL accounts for the long-term effects of physical activity on beta cells and insulin sensitivity (S_I) promoted by Interleukin-6 ($IL6$). This variable bridges the two timescales in the model. Furthermore, the state variables Γ and Σ model mechanisms that link the effects of B on the negative feedback loop between G and I [7].

A visualization of all the state variables, the control and their interplay is given in Fig. 1.

As can be seen, the coupling between the short- and long-term variables is one-way: the long-term dynamics depend on the short-term variables, but not vice versa. This one-way coupling simplifies real-world disease progression, where disease advancement, decline in stamina due to aging or comorbidities may impair physical activity habits. For further insights into the biological interpretation of this model, we make reference to the original publications [8,9] and the preceding works [5,7,25].

2.2. Existence and uniqueness

To prove existence and uniqueness of the solution we use standard arguments from the theory of ODEs. The Picard-Lindelöf theorem, which requires the right-hand side $\mathbf{f}$ in Eq. (1) to be continuous in t and Lipschitz-continuous in the state variables, guarantees local existence and uniqueness of a solution given the initial condition $\mathbf{y_0}$.

The Lipschitz-continuity with respect to the state variables can easily be verified. In System (3), the right hand sides of the short-term equations are linear in each state variable, ensuring Lipschitz-continuity. For System (4), the Lipschitz-continuity of the auxiliary functions has been established in Appendix A, which directly implies the Lipschitz-continuity of $\mathbf{f_2}(t,\mathbf{y_1},\mathbf{y_2})$.

The control $u(t)$, however, is discontinuous at time points where the Heaviside function (2) changes values, whenever $t = k\nu + \delta$ or $t = (k+1)\nu$ for $k = 0,\dots,n-1$. Despite this, in the initial interval $t \in [0,\delta]$ all the conditions for the Picard-Lindelöf theorem are satisfied and there exists a unique solution given the initial condition $\mathbf{y_0}$. For subsequent intervals, such as $t \in (\delta,\nu)$, we restart the system using the final value for $\mathbf{y}$ from the previous interval as initial condition, again yielding existence and uniqueness in the interval. By iteratively restarting the system, we extend existence and uniqueness to the entire interval $t \in [0, t_\mathrm{end}]$ for a given initial condition $\mathbf{y_0}$.

3. Model reduction for computational speedup

When numerically solving the model introduced in Section 2, the short-term equations require the numerical solver to take small time steps, in the order of minutes, to capture the periodic physical activity dynamics. Even advanced stiff solvers must resolve the periodic patterns in the short-term equations. In our experiments, enforcing a maximum step size of 1 h was necessary to ensure that the stiff solver does not skip control transitions. When simulating several years of diabetes progression, this timestep constraint results in computationally intensive simulations, especially if many repetitions are required.

Instead of passing on the short-term effects encapsulated in $\mathbf{y_1}$ to the long-term effects described in $\mathbf{y_2}$, we aim to replace these fast fluctuations with constant values that represent the average contribution of the short-term effects to $\mathbf{y_2}$. This reduction follows the idea of periodic averaging [18]. In this case, the averaging procedure can be carried out analytically due to the structure of the control function $u(t)$ and the form of the short-term dynamics.

3.1. Average solution of the short-term equations

In the interval $[0,\delta]$, where $u(t) = 1$ and $\mathbf{y_1}(0) = \mathbf{0}$, the analytical solution for System (3) is given by:

$$\mathbf{y_1}(t) = \begin{bmatrix} VO_2(t) \\ G_\mathrm{pr}(t) \\ G_\mathrm{up}(t) \\ I_\mathrm{e}(t) \\ IL6(t) \end{bmatrix} = \begin{bmatrix} 1 - e^{-\lambda_t \theta t} \\ 1 + c_1(t;\alpha_2) - c_2(t;\alpha_2) \\ 1 + c_1(t;\alpha_4) - c_2(t;\alpha_4) \\ 1 + c_1(t;\alpha_6) - c_2(t;\alpha_6) \\ 1 + c_1(t;\kappa_\mathrm{IL6}) - c_2(t;\kappa_\mathrm{IL6}) \end{bmatrix},$$

with the two auxiliary functions

$$c_1(t;\pi) := \frac{\pi}{\theta - \pi} e^{-\lambda_t \theta t} \quad \text{and} \quad c_2(t;\pi) := \frac{\theta}{\theta - \pi} e^{-\lambda_t \pi t}, \quad \text{where } \pi \neq \theta.$$

In the interval (δ,ν), where $u(t) = 0$ and the initial condition is given by evaluating the previous solution at $t = \delta$, the analytical solution for the System (3) is given by:

$$\mathbf{y_1}(t) = \begin{bmatrix} VO_2(t) \\ G_\mathrm{pr}(t) \\ G_\mathrm{up}(t) \\ I_\mathrm{e}(t) \\ IL6(t) \end{bmatrix} = \begin{bmatrix} \left(e^{\lambda_t \theta \delta} - 1\right) e^{-\lambda_t \theta t} \\ -c_3(t;\alpha_2) + c_4(t;\alpha_2) \\ -c_3(t;\alpha_4) + c_4(t;\alpha_4) \\ -c_3(t;\alpha_6) + c_4(t;\alpha_6) \\ -c_3(t;\kappa_\mathrm{IL6}) + c_4(t;\kappa_\mathrm{IL6}) \end{bmatrix},$$

where we introduce

$$c_3(t;\pi) := \left(e^{\lambda_t \theta \delta} - 1\right) c_1(t;\pi) \quad \text{and} \quad c_4(t;\pi) := \left(e^{\lambda_t \pi \delta} - 1\right) c_2(t;\pi),$$

again to write the parameters in compact form. The steps leading up to these solutions are given in Appendix C.

In the next interval, $[\nu, \nu+\delta]$, we proceed analogously, noting that $\mathbf{y_1}(\nu)$ is close to zero. Note that the four parameters α_2, α_4, α_6 and κ_IL6 are much smaller than θ (see Appendix B), such that $0 \leq \mathbf{y_1}(t) \leq 1$ holds for $t \in [0,T]$. This procedure could be continued in order to construct a semi-analytical solution of the short-term equations. This would reduce the number of ODEs required to be solved from twelve to seven. However, since these semi-analytical solutions are not constant in time, the

solver would still need to take small time steps to resolve their contribution to the slow ODEs.

Hence, we calculate the average $\boldsymbol{\mu}$ of $\mathbf{y_1}(t)$ in the interval $[0, \nu)$, defined as

$$\boldsymbol{\mu} := \frac{1}{\nu}\int_0^{\nu} \mathbf{y_1}(t)\,\mathrm{d}t = \frac{1}{\nu}\left(\int_0^{\delta} \mathbf{y_1}(t)\,\mathrm{d}t + \int_{\delta}^{\nu} \mathbf{y_1}(t)\,\mathrm{d}t\right).$$

A calculation, with details in Appendix C, yields

$$\boldsymbol{\mu} = \begin{bmatrix} \mu_{VO_2} \\ \mu_{G_{\mathrm{pr}}} \\ \mu_{G_{\mathrm{up}}} \\ \mu_{I_{\mathrm{e}}} \\ \mu_{IL6} \end{bmatrix} = \frac{1}{\nu}\begin{bmatrix} \delta + e^{-\lambda_t \theta \nu}\left(1 - e^{\lambda_t \theta \delta}\right)/(\lambda_t \theta) \\ \delta + c_\mu(\alpha_2) \\ \delta + c_\mu(\alpha_4) \\ \delta + c_\mu(\alpha_6) \\ \delta + c_\mu(\kappa_{\mathrm{IL6}}) \end{bmatrix},$$

where we introduce

$$c_\mu(\pi) := \frac{\theta}{\lambda_t \pi(\theta - \pi)} e^{-\lambda_t \pi \nu}\left(1 - e^{\lambda_t \pi \delta}\right) - \frac{\pi}{\lambda_t \theta(\theta - \pi)} e^{-\lambda_t \theta \nu}\left(1 - e^{\lambda_t \theta \delta}\right),$$

again with $\pi \neq \theta$. Note that this function is independent of t.

3.2. Reduced model

We use $\boldsymbol{\mu}$ to approximate the oscillating behavior of the short-term effects described by $\mathbf{y_1}$ and introduce an approximation $\hat{\mathbf{y}}$ to System (1):

$$\frac{\mathrm{d}}{\mathrm{d}t}\hat{\mathbf{y}}(t) = \frac{\mathrm{d}}{\mathrm{d}t}\begin{bmatrix} \hat{\mathbf{y_1}}(t) \\ \hat{\mathbf{y_2}}(t, \hat{\mathbf{y_1}}) \end{bmatrix} = \begin{bmatrix} \hat{\mathbf{f_1}}(t, \hat{\mathbf{y_1}}) \\ \mathbf{f_2}(t, \hat{\mathbf{y_1}}, \hat{\mathbf{y_2}}) \end{bmatrix} = \hat{\mathbf{f}}(t, \hat{\mathbf{y}}), \tag{5}$$

for $0 < t \leq t_{\mathrm{end}}$, together with an initial condition defined below. For $\hat{\mathbf{y_1}}$, we define a mock system

$$\frac{\mathrm{d}}{\mathrm{d}t}\hat{\mathbf{y}}_{\mathbf{1}}(t) = \frac{\mathrm{d}}{\mathrm{d}t}\begin{bmatrix} \widehat{VO_2} \\ \widehat{G_{\mathrm{pr}}} \\ \widehat{G_{\mathrm{up}}} \\ \widehat{I_{\mathrm{e}}} \\ \widehat{IL6} \end{bmatrix} = \begin{bmatrix} 0 \\ 0 \\ 0 \\ 0 \\ 0 \end{bmatrix} = \hat{\mathbf{f}}_{\mathbf{1}}(t, \hat{\mathbf{y}}_{\mathbf{1}}),$$

with the initial conditions $\hat{\mathbf{y}}_{\mathbf{1}}(0) := \boldsymbol{\mu}$. The right hand side for $\hat{\mathbf{y}}_{\mathbf{2}}$ remains as written out in System (4), but now gets the inputs from $\hat{\mathbf{y}}_{\mathbf{1}}$:

$$\frac{\mathrm{d}}{\mathrm{d}t}\hat{\mathbf{y}}_{\mathbf{2}} = \frac{\mathrm{d}}{\mathrm{d}t}\begin{bmatrix} \widehat{VL} \\ \hat{S}_{\mathrm{I}} \\ \hat{\Gamma} \\ \hat{\Sigma} \\ \hat{B} \\ \hat{I} \\ \hat{G} \end{bmatrix} = \begin{bmatrix} h_{VL}(\widehat{VL}, \widehat{IL6}) \\ h_{S_{\mathrm{I}}}(\hat{S}_{\mathrm{I}}, \widehat{VL}) \\ h_{\Gamma}(\hat{\Gamma}, \hat{G}) \\ h_{\Sigma}(\hat{\Sigma}, \hat{\Gamma}, \hat{G}) \\ h_B(\hat{B}, \widehat{VL}, \hat{\Gamma}, \hat{\Sigma}, \hat{G}) \\ h_I(\hat{I}, \hat{I}_{\mathrm{e}}, \hat{\Gamma}, \hat{\Sigma}, \hat{B}, \hat{G}) \\ h_G(\hat{G}, \widehat{G_{\mathrm{up}}}, \widehat{G_{\mathrm{pr}}}, \hat{S}_{\mathrm{I}}, \hat{I}) \end{bmatrix} = \mathbf{f_2}(t, \hat{\mathbf{y}}_{\mathbf{1}}, \hat{\mathbf{y}}_{\mathbf{2}}), \tag{6}$$

with the previously given initial conditions. Note that $\hat{\mathbf{y}}(t)$ no longer directly depends on $u(t)$, because the control only influences the system via its parameters. The existence and uniqueness of solutions to System (5) directly follows from the existence and uniqueness shown in Section 2.2. From a numerical perspective, it is not necessary to solve System (5) explicitly. Instead, we can directly solve System (6), using the fact that $\hat{\mathbf{y}}_{\mathbf{1}}(t) = \boldsymbol{\mu}$ for $0 \leq t \leq t_{\mathrm{end}}$.

In classical homogenization and averaging theory, the separation of scales is typically introduced through a small parameter ε such that fast dynamics evolve on the scaled time t/ε. In our formulation, the constant parameter λ_t plays a similar role to $1/\varepsilon$. To stay consistent with the physiological interpretation of the model, we keep the notation λ_t and do not study the asymptotic limit $\lambda_t \to \infty$. Instead, we focus on a practical reduction of the system for fixed values of λ_t, relevant to the long-term effects of regular physical activity.

3.3. Approximation error

We show that the error introduced by the homogenization procedure is bounded over a finite time horizon, for a fixed separation of timescales determined by the parameter λ_t. Rather than analyzing the asymptotic limit, we quantify the approximation at physiologically relevant parameter values. To this end, we define the vector-valued L^∞ norm as follows:

$$\|\mathbf{g}\|_{L^\infty([0,t_{\mathrm{end}}])} = \max_{i=1,\dots,m}\left\{\operatorname*{ess\,sup}_{t\in[0,t_{\mathrm{end}}]} |g_i(t)|\right\}$$

for a function $\mathbf{g} \in L^\infty([0, t_{\mathrm{end}}], \mathbb{R}^m)$. This error reflects the largest deviation across all state variables over the time horizon.

Theorem 1. *Let $\mathbf{y}(t, u)$ as introduced in System (1) and $\hat{\mathbf{y}}(t)$ as introduced in System (5). Then there exists a constant C depending on t_{end} such that*

$$\|\mathbf{y}(t, u) - \hat{\mathbf{y}}(t)\|_{L^\infty([0,t_{\mathrm{end}}])} \leq C(t_{\mathrm{end}}).$$

Proof. We can split the error as follows:

$$\|\mathbf{y}(t, u) - \hat{\mathbf{y}}(t)\|_{L^\infty([0,t_{\mathrm{end}}])} = \max\left\{\|\mathbf{y_1}(t, u) - \hat{\mathbf{y}}_{\mathbf{1}}(t)\|_{L^\infty([0,t_{\mathrm{end}}])}, \|\mathbf{y_2}(t, \mathbf{y_1}) - \hat{\mathbf{y}}_{\mathbf{2}}(t, \hat{\mathbf{y}}_{\mathbf{1}})\|_{L^\infty([0,t_{\mathrm{end}}])}\right\}.$$

Since $\hat{\mathbf{y}}_{\mathbf{1}}(t) = \boldsymbol{\mu}$ by construction, we can bound the first part directly:

$$\|\mathbf{y_1}(t, u) - \hat{\mathbf{y}}_{\mathbf{1}}(t)\|_{L^\infty([0,t_{\mathrm{end}}])} = \|\mathbf{y_1}(t, u) - \boldsymbol{\mu}\|_{L^\infty([0,t_{\mathrm{end}}])} = \|1 - \boldsymbol{\mu}\|_{L^\infty},$$

where we used that $\mathbf{y_1}(t, u) \in [0, 1]$ due to the scaling and that every element of $\boldsymbol{\mu}$ is smaller than 0.5. In the L^∞-norm, this error is independent of t_{end} by construction, but larger than it would be in L^2-norm for example.

For the second part, we first note that

$$\begin{aligned}\|\mathbf{f_2}(t, \mathbf{y_1}, \mathbf{y_2}) - \mathbf{f_2}(t, \hat{\mathbf{y}}_{\mathbf{1}}, \hat{\mathbf{y}}_{\mathbf{2}})\|_{L^\infty([0,t_{\mathrm{end}}])} \leq& \mathbf{L_1}\|\mathbf{y_1} - \hat{\mathbf{y}}_{\mathbf{1}}\|_{L^\infty([0,t_{\mathrm{end}}])} \\ &+ \mathbf{L_2}\|\mathbf{y_2} - \hat{\mathbf{y}}_{\mathbf{2}}\|_{L^\infty([0,t_{\mathrm{end}}])} \\ \leq& \mathbf{L_1}\|1 - \boldsymbol{\mu}\|_{L^\infty} \\ &+ \mathbf{L_2}\|\mathbf{y_2} - \hat{\mathbf{y}}_{\mathbf{2}}\|_{L^\infty([0,t_{\mathrm{end}}])}.\end{aligned}$$

with Lipschitz constants $\mathbf{L_1}$ and $\mathbf{L_2}$. This holds by definition of the Lipschitz-continuity of $\mathbf{f_2}$. We now invoke the Grönwall-Lemma in its differential form to bound $\|\mathbf{y_2}(t, \mathbf{y_1}) - \hat{\mathbf{y}}_{\mathbf{2}}(t, \hat{\mathbf{y}}_{\mathbf{1}})\|_{L^\infty([0,t_{\mathrm{end}}])}$ and get that

$$\|\mathbf{y_2}(t, \mathbf{y_1}) - \hat{\mathbf{y}}_{\mathbf{2}}(t, \hat{\mathbf{y}}_{\mathbf{1}})\|_{L^\infty([0,t_{\mathrm{end}}])} \leq \mathbf{L_1}\|1 - \boldsymbol{\mu}\|_{L^\infty}\int_0^t e^{\mathbf{L_2}(t-s)}\,\mathrm{d}s,$$

for $t \in [0, t_{\mathrm{end}}]$. A calculation yields

$$\begin{aligned}\|\mathbf{y_2}(t, \mathbf{y_1}) - \hat{\mathbf{y}}_{\mathbf{2}}(t, \hat{\mathbf{y}}_{\mathbf{1}})\|_{L^\infty([0,t_{\mathrm{end}}])} &\leq \mathbf{L_1}\|1 - \boldsymbol{\mu}\|_{L^\infty} e^{\mathbf{L_2}t}\int_0^t e^{-\mathbf{L_2}s}\,\mathrm{d}s \\ &= \frac{\mathbf{L_1}}{\mathbf{L_2}}\|1 - \boldsymbol{\mu}\|_{L^\infty}\left(e^{\mathbf{L_2}t} - 1\right)\end{aligned}$$

for $t \in [0, t_{\mathrm{end}}]$. It follows that

$$\|\mathbf{y}(t, u) - \hat{\mathbf{y}}(t)\|_{L^\infty([0,t_{\mathrm{end}}])} \leq C(t_{\mathrm{end}}).$$

□

A related proof can be found in Sanders et al. [18, Section 2.8], which presents a classical averaging result in the asymptotic regime $\varepsilon \to 0$. In contrast, our setting assumes a fixed separation of timescales via the parameter $\lambda_t \sim 1/\varepsilon$. Rather than analyzing the asymptotic limit, we aim to establish a practical error bound for physiologically relevant values of λ_t over a finite time horizon. The bound in Theorem 1 therefore depends on t_{end} and reflects the cumulative effect of replacing the periodic short-term dynamics with their average.

4. Numerical results

The reduced model provides a significant computational speedup compared to the full model, as it does not require resolving minute-scale dynamics. This allows the numerical solver to take time steps on the order of days rather than minutes. Furthermore, the numerical results underline that the two systems behave very similarly, as presented in the following.

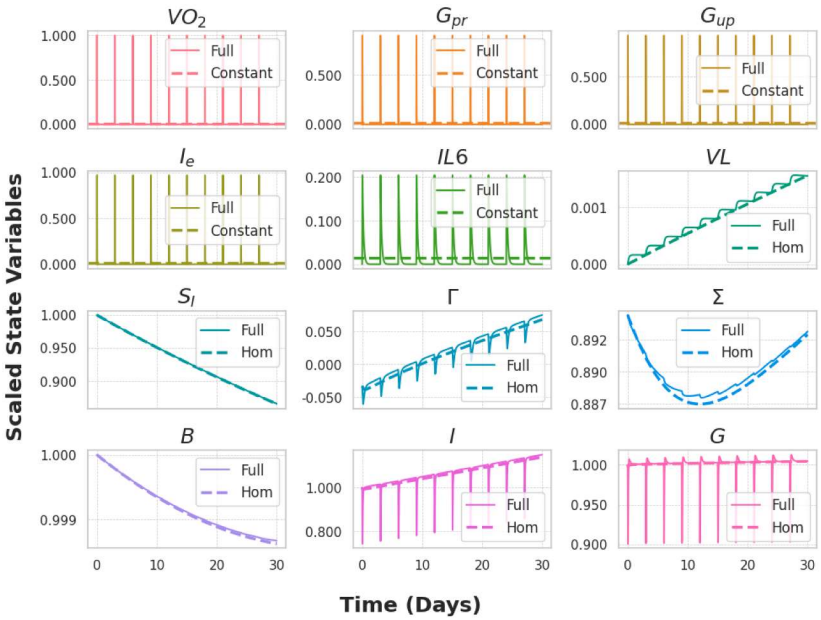

Fig. 2. Illustration of the numerical solution of the full model (solid lines) and the reduced model (dashed lines) for all 12 state variables for one month. All the parameters are chosen as outlined in Appendix B.

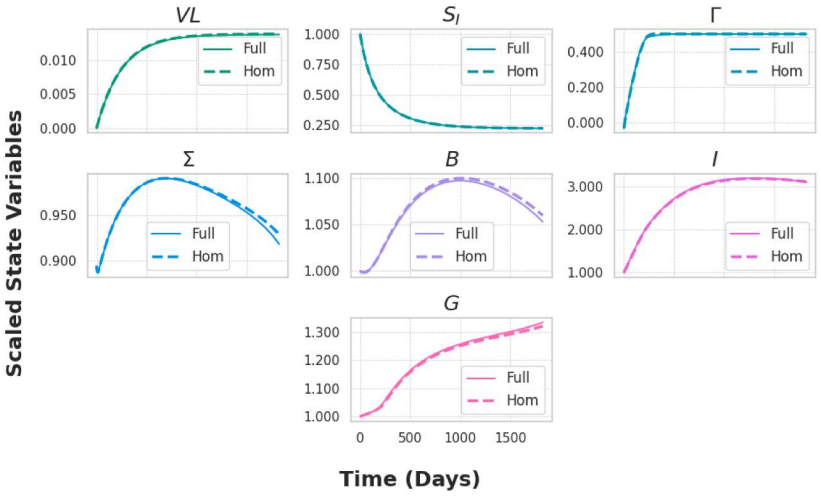

Fig. 3. Solution at basal times (moments of the start of physical activity) of the full model (solid lines) and the reduced model (dashed) for five years. All the parameters are chosen as outlined in Appendix B.

4.1. Illustration

System (1) with the standard parameters listed in Appendix B is stiff. To numerically solve it, we use a fifth-order implicit Runge-Kutta method and constrain the step size of a maximum of 1 h to not skip the control transitions at the start and end of a physical activity session. An illustration of the numerical solutions for one month of the full and the reduced model can be found in Fig. 2.

To examine the long-term behavior of both the full and the reduced model, we focus on the solutions at basal times, referring to the moments of the start of physical activity. Fig. 3 presents the solutions over a five-year period.

4.2. Simulation study

To assess the speedup and the approximation error made by reducing the system, we vary six parameters and three initial conditions, resulting in 19 683 parameter configurations, and simulate the full and the reduced model over a 5-year period. Following the definition of the approximation error in Section 3.3, we define the maximal deviation at basal times between the two systems over 5 years for simulation i as E_i^{basal}. This metric captures the largest discrepancy between the two systems and thus provides a conservative upper bound on the approximation error. We also consider the pointwise error at 5 years, E_i^{5y}. Since classification into normoglycemia or type 2 diabetes is based on glucose thresholds, we use E_i^{5y} to check whether the reduced model does not incorrectly classify subjects as normoglycemic when the full model would indicate type 2 diabetes. Details on the parameters and the error measures can be found in Appendix D. All simulations were performed using the `solve_ivp` implementation with `method = 'Radau'` from the `scipy` package on a computing server equipped with a 64 core AMD EPYC 7763 CPU and one Nvidia GeForce RTX 4090 GPU.

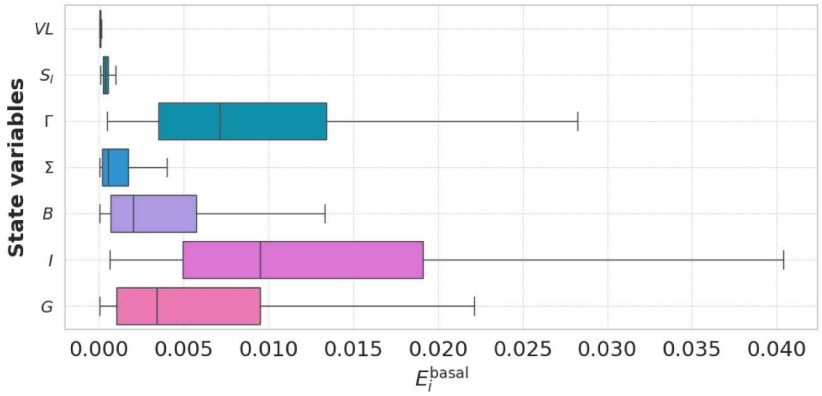

Fig. 4. Box plot showing the distribution of the maximal deviation E_i^{basal} between the full and the reduced model across 19 683 simulations.

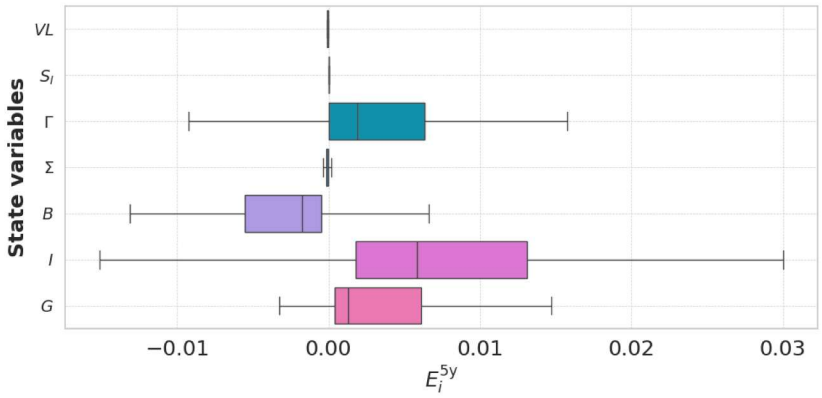

Fig. 5. Box plot showing the distribution of the deviation E_i^{5y} between the full and the reduced model across 19 683 simulations at 5 years.

On average, simulating the full model over a five-year period with a stiff solver (Radau) requires 98 s (SD 26 s). The reduced model requires no constraint on the step size, resulting in a substantial computational speedup. On average, one simulation over the five-year period takes 0.053 s (SD 0.01 s), corresponding to a reduction in computational time of a factor 1914 (SD 655). This slighlty exceeds the theoretically expected speedup factor of $\lambda_t = 1440$, reflecting the relationship between the two timescales.

A box plot summarizing the distribution of E_i^{basal} across the 19 683 simulations is shown in Fig. 4.

These findings underline that the maximal error across the simulations remains reasonably small. A box plot summarizing the distribution of E_i^{5y} across the 19 683 simulations is given in Fig. 5.

The pointwise error of glucose G at 5 years is small and negative in only 5 out of 19 683 simulations. This confirms that the reduced model closely approximates the full model while achieving a λ_t-fold speedup. Furthermore, the risk of misclassification based on glucose values is minimal.

5. Discussion

In this work, we developed and analyzed a reduced, computationally efficient version of a two-scale model capturing the long-term effects of physical activity on blood glucose regulation. The reduced model retains the essential dynamics of the original formulation while decreasing the computational cost of simulating multi-year trajectories to type 2 diabetes. This gain in efficiency allows for extensive patient-specific simulations and the systematic evaluation of physical activity plans in a personalized context.

The computational speedup was achieved by analytically reducing the original model using the periodic nature of the physical activity input (control variable u). We analytically solved the short-term effects of physical activity and passed them to the long-term dynamics as averaged quantities. By treating the reduction as a perturbation of the right-hand side, we proved that the approximation error remains bounded. These results are underlined with a simulation study where nine key parameters were varied. This confirmed that the reduced model reproduces the full model's dynamics with negligible long-term discrepancies. The resulting model lowers the simulation time of a five-year trajectory by almost a factor 2000. Indeed, simulating a single parameter set over a five-year period takes around 0.05 s, making the fast simulation of many scenarios feasible.

The proposed formulation was designed to solve the original system with minimal computational effort while maintaining accuracy. Alternative simplifications, such as using semi-analytical solutions of the short-term equations directly or replacing the physical activity input with a constant average input, would still require the numerical solver to take small time steps to resolve the oscillations. In contrast, the proposed formulation removes these fast variations analytically, allowing the solver to take large time steps (i.e., days instead of minutes) and achieve a significant computational speedup, while retaining the physiologically meaningful link between exercise and glucose regulation.

We established formal existence and uniqueness results and introduced a scaled formulation that improves numerical stability. The

reduction approach draws on concepts from homogenization theory but departs from its classical asymptotic framework, which typically examines model behavior as the timescale separation tends to infinity [18,19]. In contrast, the proposed formulation assumes a fixed, physiologically meaningful separation of timescales and evaluates how accurately the reduced model reproduces the full system over a realistic five-year horizon. A more formal asymptotic analysis based on averaging theory and including convergence results would be a valuable direction for future work.

This model formulation can only describe the physiological mechanisms explicitly included. As with previous formulations [8,9], the model describes an average patient at risk of developing type 2 diabetes. Individual differences can be captured through several patient-specific parameters, including insulin sensitivity. Other factors, such as age, sex, family history of type 2 diabetes and dietary patterns, which might also confound the physical activity adherence, are not explicitly parametrized, but are partially embedded in the inter-individual parameter variability, as detailed in previous work [9]. While the patient-specific parameters can capture a range of intrinsic patient differences, several important physiological and pathological processes remain beyond the current model scope. The model does not encapsulate the interplay with potential comorbidities, such as infectious diseases and non-communicable diseases. Also, for simulating longer periods than a 5-year-window, age-dependent stamina decline should also be accounted for. Incorporating these mechanisms would, however, increase the structural and numerical complexity of the model, which is already high due to the nonlinear interaction terms driving the glucose-insulin dynamics [26,27].

While this model has not been validated against longitudinal datasets tracking the long-term effects of physical activity on type 2 diabetes progression, partial validation of the full model has been achieved. Specifically, it has been tested against data extracted from the literature, including the average effects of physical activity and the influence of inter-individual variability modeled through parameter perturbations [9]. The resulting predictions are consistent with existing knowledge and real-world evidence. Nevertheless, comprehensive validation against large-scale, long-term exercise datasets remains limited due to challenges in capturing multi-year adherence, frequency, and intensity of physical activity. Such validation might become feasible with wearable technologies generating high-frequency, longitudinal data for robust calibration.

The considerable reduction in computational effort allows for the applicability of the reduced model in the field of medical decision support. Personalized physical activity plans, along with uncertainty quantification, can now be evaluated efficiently, for example in a Bayesian framework requiring thousands of model evaluations to characterize posterior distributions. This model has already been integrated into a causal framework to assess the impact of hypothetical physical activity plans in slowing down or preventing progression to type 2 diabetes in at-risk individuals [28]. In this work, we used a structural causal model based on the dynamics of this reduced model, to analyze the impact of tailored physical activity recommendations on the 5-year-prevention of type 2 diabetes onset, in individuals with prediabetes. The computational efficiency of the model enabled the generation of a broad set of simulations in limited time, thereby allowing counterfactual inference to be performed with tractable computational complexity. The results from this work can be used as a basis to provide clinicians with patient-specific what-if analyses and support personalized decision-making in clinical settings.

Future extensions of the full model should incorporate dietary patterns as time-varying control inputs affecting glucose production. In its present form, the model assumes an average dietary intake, that can be manipulated to modify overall intake and modulate the balance between training and diet. More detailed formulations could explicitly account for the effects of nutritional intake on model parameters, as diet modulates both metabolic rates and training efficacy, at the expense of increased complexity. Also, feedback loops affecting the physical activity profiles due to stamina decline or comorbidities represent another promising direction, where homogenization theory could be applied to more complex model structures.

In summary, this work introduces a mathematically grounded and computationally efficient formulation of a physiologically detailed glucose regulation model. By leveraging homogenization principles, we achieve a reduction that enables fast, accurate long-term simulations and extends the model's usability to personalized type 2 diabetes risk prediction. More broadly, this approach illustrates how mechanistic models in systems biology can benefit from mathematical reduction and analysis techniques to achieve both rigor and scalability.

6. Code availability

The code supporting this work is publicly available at:
https://gitlab-core.supsi.ch/dti-idsia/Homogen_ODEs_T2D

CRediT authorship contribution statement

Lea Multerer: Writing – review & editing, Writing – original draft, Visualization, Software, Methodology, Formal analysis, Conceptualization; **Pierluigi Francesco De Paola:** Writing – review & editing, Methodology, Investigation; **Marta Lenatti:** Writing – review & editing, Methodology, Investigation; **Alessia Paglialonga:** Writing – review & editing, Methodology, Investigation, Funding acquisition, Conceptualization; **Laura Azzimonti:** Writing – review & editing, Supervision, Methodology, Investigation, Funding acquisition, Formal analysis, Conceptualization.

Data availability

No data was used for the research described in the article.

Declaration of competing interest

The authors declare that they have no known competing financial interests or personal relationships that could have appeared to influence the work reported in this paper.

Acknowledgment

This work was supported by the European Union and by the Swiss State Secretariat for Education, Research and Innovation (SERI) through project PRAESIIDIUM "Physics informed machine learning-based prediction and reversion of impaired fasting glucose management" under Grant 101095672. Views and opinions expressed are however those of the authors only and do not necessarily reflect those of the European Union and SERI. The European Union and SERI cannot be held responsible for them.

Pierluigi Francesco De Paola is a PhD student enrolled in the National PhD Program in Autonomous Systems (DAUSY), coordinated by Politecnico of Bari, Bari, Italy.

Marta Lenatti is a PhD student enrolled in the National PhD in Artificial Intelligence, XXXVIII cycle, course on Health and life sciences, organized by Università Campus Bio-Medico di Roma.

The authors thank Fabrizio Dabbene, Alessandro Borri and Pasquale Palumbo for their valuable discussions about the full model.

Appendix A. Scaling of the model

We adopt the following notation: state variables are represented by capital letters, using either Greek or Latin characters. Parameters, which are always constant in time, are consistently denoted by lowercase Greek letters and may include subscripts. Functions are written as lowercase Latin letters, and also may include subscripts.

A.1. Scaling of the short-term equations

We rescale the original system [8,9] based on the magnitude of the state variables and introduce a unified timescale. The equations on a minute-scale read

$$\begin{aligned}
\frac{\mathrm{d}}{\mathrm{d}t} VO_2 &= \theta u(t) - \theta VO_2,\\
\frac{\mathrm{d}}{\mathrm{d}t} G_{\mathrm{pr}} &= \alpha_1 VO_2 - \alpha_2 G_{\mathrm{pr}},\\
\frac{\mathrm{d}}{\mathrm{d}t} G_{\mathrm{up}} &= \alpha_3 VO_2 - \alpha_4 G_{\mathrm{up}},\\
\frac{\mathrm{d}}{\mathrm{d}t} I_{\mathrm{e}} &= \alpha_5 VO_2 - \alpha_6 I_{\mathrm{e}},\\
\frac{\mathrm{d}}{\mathrm{d}t} IL6 &= \kappa_{\mathrm{SR}} VO_2 - \kappa_{\mathrm{IL6}} IL6,\\
\frac{\mathrm{d}}{\mathrm{d}t} VL &= IL6 - \kappa_{\mathrm{s}} VL,
\end{aligned}$$

with the initial conditions being 0 for all the equations. The control $u(t)$ is introduced as

$$u(t) = \begin{cases} \xi & \text{for } 0 \le t \le \text{duration (min)},\\ 0 & \text{for duration (min)} < t < \text{period length (min)}, \end{cases}$$

where ξ is the physical activity intensity. The period length refers to the time between the start of two consecutive physical activity sessions. Note that the state variable VL is included in this set of equations because it was originally parameterized in minutes and hence requires the short-term scaling. However, since it has a long-term effect we will include it in the long-term equations for the homogenization further below.

The original units of the state variables, along with their description, are given in Table A.1.

Table A.1
Short description and units of the short-term state variables in their unscaled form.

Variable	Description	Unit
VO_2	Oxygen consumption during exercise	given in %
G_{pr}	Incremental hepatic glucose production	mg/(kg min)
G_{up}	Increased glucose uptake by working tissues	mg/(kg min)
I_{e}	Incremental insulin removal	μU/ml
$IL6$	Concentration of IL-6 in the muscle	pg/ml
VL	Integral effect of IL-6 released during exercise	(pg/ml) min

To solve these ODEs simultaneously with the long-term equations defined at a daily timescale, we first convert the short-term equations to days. Additionally, we scale the state variables to be dimensionless. Following standard procedures for the scaling of ODEs [24], we introduce

$$\bar{t} := \frac{t}{\lambda_t} \text{ and } \overline{\Omega} := \frac{\Omega}{\lambda_\Omega},\ \Omega \in \{t, VO_2, G_{\mathrm{pr}}, G_{\mathrm{up}}, I_{\mathrm{e}}, IL6, VL\}.$$

Substituting into both sides of the unscaled system and rearranging yields

$$\begin{aligned}
\frac{\mathrm{d}}{\mathrm{d}\bar{t}} \overline{VO_2} &= \lambda_t \left(\frac{\theta}{\lambda_{VO_2}} u(\lambda_t \bar{t}) - \theta \overline{VO_2} \right),\\
\frac{\mathrm{d}}{\mathrm{d}\bar{t}} \overline{G_{\mathrm{pr}}} &= \lambda_t \left(\frac{\alpha_1 \lambda_{VO_2}}{\lambda_{G_{\mathrm{pr}}}} \overline{VO_2} - \alpha_2 \overline{G_{\mathrm{pr}}} \right),\\
\frac{\mathrm{d}}{\mathrm{d}\bar{t}} \overline{G_{\mathrm{up}}} &= \lambda_t \left(\frac{\alpha_3 \lambda_{VO_2}}{\lambda_{G_{\mathrm{up}}}} \overline{VO_2} - \alpha_4 \overline{G_{\mathrm{up}}} \right),\\
\frac{\mathrm{d}}{\mathrm{d}\bar{t}} \overline{I_{\mathrm{e}}} &= \lambda_t \left(\frac{\alpha_5 \lambda_{VO_2}}{\lambda_{I_{\mathrm{e}}}} \overline{VO_2} - \alpha_6 \overline{I_{\mathrm{e}}} \right),\\
\frac{\mathrm{d}}{\mathrm{d}\bar{t}} \overline{IL6} &= \lambda_t \left(\frac{\kappa_{\mathrm{SR}} \lambda_{VO_2}}{\lambda_{IL6}} \overline{VO_2} - \kappa_{\mathrm{IL6}} \overline{IL6} \right),\\
\frac{\mathrm{d}}{\mathrm{d}\bar{t}} \overline{VL} &= \lambda_t \left(\frac{\lambda_{IL6}}{\lambda_{VL}} \overline{IL6} - \kappa_{\mathrm{s}} \overline{VL} \right).
\end{aligned}$$

The initial conditions are 0 for all equations, hence no scaling is necessary. We now select the scaling constants as specified in Appendix B. Note that the choice of λ_t transforms the time from minutes to days. All the other constants are chosen to make the state variables unitless and to scale the system to take values in the interval $[0, 1]$. We conclude the scaling of the short-term state variables by noting that, to include them in the long-term equations, they must be rescaled to their original units. In particular, state variables with minute-based units must be converted to days as follows:

$$G_{\mathrm{pr}}^{\mathrm{day}} := \lambda_t G_{\mathrm{pr}},\ G_{\mathrm{up}}^{\mathrm{day}} := \lambda_t G_{\mathrm{up}},\ VL^{\mathrm{day}} := \frac{VL}{\lambda_t}.$$

A.2. Auxiliary functions for the long-term equations

We provide a concise overview of the set of auxiliary functions originally introduced in the appendix of the publication by Ha et al. [7]. We first define the two functions q_h and q_e as follows:

$$\begin{aligned}
q_h(x; \pi_1, \pi_2) &:= \frac{x^{\pi_2}}{x^{\pi_2} + \pi_1^{\pi_2}}, \text{ for } \pi_1 \in \mathbb{R}^+,\ \pi_2 \in 2\mathbb{N}^+,\\
q_e(x; \pi_1, \pi_2, \pi_3, \pi_4) &:= \frac{\pi_1}{1 + \pi_4 e^{-(x-\pi_2)/\pi_3}} \text{ for } \pi_1, \pi_2, \pi_3, \pi_4 \in \mathbb{R}^+,
\end{aligned}$$

where $x \in \mathbb{R}$. Under the listed constraints on the constants, both functions are Lipschitz-continuous and bounded in x. With these functions at hand, we define the following auxiliary functions, following the notation of the original publications wherever possible. A list of all the parameters introduced here can be found in Appendix B. The first set of functions is based on the Hill-type function q_h:

$$\begin{aligned}
m(G) &= q_h(G; \alpha_{\mathrm{M}}, 2),\\
r(\Gamma, \Sigma, G) &= \Sigma q_h\big(m(G) + \Gamma; \alpha_{\mathrm{ISR}}, 2\big),\\
p(VL, \Gamma, \Sigma, G) &= \phi_{\max} q_h\big(r(\Gamma, \Sigma, G); \alpha_{\mathrm{P}}, 4\big)\big(1 + \zeta_1 q_h(VL; \kappa_{\mathrm{n}}, 2)\big),\\
a(VL, G) &= \Big(\alpha_{\max} q_h\big(m(G); \alpha_{\mathrm{A}}, 6\big) + \alpha_{\mathrm{B}}\Big)\Big(1 - \zeta_2 q_h(VL; \kappa_{\mathrm{n}}, 2)\Big).
\end{aligned}$$

It can be shown that all of these functions are Lipschitz-continuous with respect to all of their arguments. Furthermore, it can be verified that the functions m, p and a are bounded. The function r is only bounded if Σ is bounded.

The second set requires the function q_e:

$$\begin{aligned}
g_\infty(G) &= q_e(G; \gamma_{\max}, \gamma_{\mathrm{S}}, \gamma_{\mathrm{n}}, 1) - \gamma_\theta,\\
s_{\mathrm{ISR}\infty}(\Gamma, \Sigma, G) &= q_e\big(r(\Gamma, \Sigma, G - \kappa_{\sigma\mathrm{s}}); \sigma_{\mathrm{ISRmax}}, \sigma_{\mathrm{ISRs}}, \sigma_{\mathrm{ISRn}}, \sigma_{\mathrm{ISRk}}\big),\\
s_{\mathrm{M}\infty}(G) &= 1 - q_e\big(m(G - \kappa_{\sigma\mathrm{s}}); \sigma_{\mathrm{Mmax}}, \sigma_{\mathrm{Ms}}, \sigma_{\mathrm{Mn}}, \sigma_{\mathrm{Mk}}\big),\\
s_\infty(\Gamma, \Sigma, G) &= s_{\mathrm{ISR}\infty}(\Gamma, \Sigma, G) s_{\mathrm{M}\infty}(G) + \sigma_{\mathrm{B}}.
\end{aligned}$$

Again, it is clear that all of these functions are Lipschitz-continuous and bounded in all of their arguments, as long as all of the parameters are positive.

A.3. Scaling of the long-term equations

The long-term equations are written down in the original publication as follows:

$$\begin{aligned}
\frac{\mathrm{d}}{\mathrm{d}t} S_{\mathrm{I}} &= \left(\frac{\theta_{S_{\mathrm{I}}} - S_{\mathrm{I}}}{\tau_{S_{\mathrm{I}}}} \right) \left(1 - \zeta_3 \frac{VL^{\mathrm{day}}}{k_{nS_{\mathrm{I}}} + VL^{\mathrm{day}}} \right),\\
\frac{\mathrm{d}}{\mathrm{d}t} \Gamma &= \frac{g_\infty(G) - \Gamma}{\tau_\Gamma},\\
\frac{\mathrm{d}}{\mathrm{d}t} \Sigma &= \frac{s_\infty(\Gamma, \Sigma, G) - \Sigma}{\tau_\Sigma},\\
\frac{\mathrm{d}}{\mathrm{d}t} B &= \frac{p(VL^{\mathrm{day}}, \Gamma, \Sigma, G) - a(VL^{\mathrm{day}}, G)}{\tau_B} B,\\
\frac{\mathrm{d}}{\mathrm{d}t} I &= \frac{r(\Gamma, \Sigma, G)}{\upsilon} B - \kappa I - I_{\mathrm{e}},\\
\frac{\mathrm{d}}{\mathrm{d}t} G &= \rho_0 + \frac{\omega}{\upsilon_g}(G_{\mathrm{pr}}^{\mathrm{day}} - G_{\mathrm{up}}^{\mathrm{day}}) - (\eta_0 + S_{\mathrm{I}} I) G,
\end{aligned}$$

Table A.2
Short description and units of the long-term state variables in their unscaled form.

Variable	Description	Unit
S_I	Insulin sensitivity	ml/(μU day)
Γ	Shift of the glucose dependence	–
Σ	Insulin secretion capacity	μU/ (μg day)
B	Beta cell mass	mg
I	Serum insulin concentration	μU/ml
G	Plasma glucose concentration	mg/dl

with initial conditions $S_\mathrm{I}(0) = S_{\mathrm{I}0}$, $\Gamma(0) = \Gamma_0$, $\Sigma(0) = \Sigma_0$, $B(0) = B_0$, $I(0) = I_0$ and $G(0) = G_0$. The five auxiliary functions g_∞, s_∞, p, a and r have been defined above. The original units of the introduced long-term state variables, along with their description, are given in Table A.2.

Again, we introduce the following scaling of the state variables

$$\overline{\Omega} := \frac{\Omega}{\lambda_\Omega}, \ \Omega \in \{S_\mathrm{I}, \Gamma, \Sigma, B, I, G\}.$$

The chosen scaling parameters, along with all the parameters introduced, are listed in Appendix B. Note that t does not require scaling since we want to solve the final system in days. For simplification, we introduce the following auxiliary functions:

$$\begin{aligned}
d_\lambda(\overline{VL}) &:= \frac{1}{\lambda_{S_\mathrm{I}}}\left(1 - \zeta_3\left(\frac{(\lambda_{VL}/\lambda_t)\overline{VL}}{\kappa_{\mathrm{n}S_\mathrm{I}} + (\lambda_{VL}/\lambda_t)\overline{VL}}\right)\right),\\
g_\lambda(\overline{G}) &:= \frac{1}{\lambda_\Gamma} g_\infty(\lambda_G \overline{G}),\\
s_\lambda(\overline{\Gamma}, \overline{\Sigma}, \overline{G}) &:= \frac{1}{\lambda_\Sigma} s_\infty(\lambda_\Gamma \overline{\Gamma}, \lambda_\Sigma \overline{\Sigma}, \lambda_G \overline{G})\\
p_\lambda(\overline{VL}, \overline{\Gamma}, \overline{\Sigma}, \overline{G}) &:= p((\lambda_{VL}/\lambda_t)\overline{VL}, \lambda_\Gamma \overline{\Gamma}, \lambda_\Sigma \overline{\Sigma}, \lambda_G \overline{G}),\\
a_\lambda(\overline{VL}, \overline{G}) &:= a((\lambda_{VL}/\lambda_t)\overline{VL}, \lambda_G \overline{G}),\\
r_\lambda(\overline{\Gamma}, \overline{\Sigma}, \overline{G}) &:= \frac{\lambda_B}{\lambda_I \upsilon} r(\lambda_\Gamma \overline{\Gamma}, \lambda_\Sigma \overline{\Sigma}, \lambda_G \overline{G}).
\end{aligned} \tag{A.1}$$

We furthermore define the following constants:

$$\lambda_{I_\mathrm{e}I} := \frac{\lambda_{I_\mathrm{e}}}{\lambda_I}, \quad \rho_\lambda := \frac{\rho_0}{\lambda_G}, \quad \lambda_{tG} := \frac{\lambda_t}{\lambda_G \upsilon_g}, \quad \lambda_{S_\mathrm{I}I} := \lambda_{S_\mathrm{I}} \lambda_I.$$

After substituting the scaling parameters and rewriting, we obtain the following system of ODEs:

$$\begin{aligned}
\frac{\mathrm{d}}{\mathrm{d}t}\overline{S_\mathrm{I}} &= d_\lambda(\overline{VL})\left(\frac{\theta_{S_\mathrm{I}} - \lambda_{S_\mathrm{I}}\overline{S_\mathrm{I}}}{\tau_{S_\mathrm{I}}}\right),\\
\frac{\mathrm{d}}{\mathrm{d}t}\overline{\Gamma} &= \frac{g_\lambda(\overline{G}) - \overline{\Gamma}}{\tau_\Gamma},\\
\frac{\mathrm{d}}{\mathrm{d}t}\overline{\Sigma} &= \frac{s_\lambda(\overline{\Gamma}, \overline{\Sigma}, \overline{G}) - \overline{\Sigma}}{\tau_\Sigma},\\
\frac{\mathrm{d}}{\mathrm{d}t}\overline{B} &= \frac{p_\lambda(\overline{VL}, \overline{\Gamma}, \overline{\Sigma}, \overline{G}) - a_\lambda(\overline{VL}, \overline{G})}{\tau_B}\overline{B},\\
\frac{\mathrm{d}}{\mathrm{d}t}\overline{I} &= r_\lambda(\overline{\Gamma}, \overline{\Sigma}, \overline{G})\overline{B} - \kappa\overline{I} - \lambda_{I_\mathrm{e}I}\overline{I_\mathrm{e}},\\
\frac{\mathrm{d}}{\mathrm{d}t}\overline{G} &= \rho_\lambda + \lambda_{tG}\omega(\lambda_{G_\mathrm{pr}}\overline{G_\mathrm{pr}} - \lambda_{G_\mathrm{up}}\overline{G_\mathrm{up}}) - (\eta_0 + \lambda_{S_\mathrm{I}I}\overline{S_\mathrm{I}I})\overline{G},
\end{aligned}$$

together with the initial conditions $S_\mathrm{I}(0) = 1$, $\Gamma(0) = \Gamma_0/\gamma_{\max} =: \Gamma_{0\lambda}$, $\Sigma(0) = \Sigma_0/\sigma_{\mathrm{ISR}\max} =: \Sigma_{0\lambda}$, $B(0) = 1$, $I(0) = 1$ and $G(0) = 1$.

Appendix B. Parameters

All parameters in this appendix are taken from the full model publications [8,9] and the references therein. A list of the parameters introduced in the short-term equations ($\mathbf{y_1}$) can be found in Table B.1.

Table B.1
Parameters related to the control $u(t)$ (top), the system of ODEs for $\mathbf{y_1}$ (middle) and the scaling of $\mathbf{y_1}$ (bottom). Standard values or the formula and the respective units are given in columns 2 and 3 [8,9].

Parameter	Definition	Unit
ν	3	day
δ	60/1440	day
ξ	50	%
θ	0.8	1/min
α_1	0.00158	mg/(kg min^2)
α_2	0.056	1/min
α_3	0.00195	mg/(kg min^2)
α_4	0.0485	1/min
α_5	0.00125	μU/(ml min)
α_6	0.075	1/min
κ_{SR}	0.045	pg/(ml min)
κ_{IL6}	0.004	1/min
λ_t	1440	min/day
λ_{VO_2}	ξ	given in %
λ_{G_pr}	$\lambda_{VO_2}\alpha_1/\alpha_2$	mg/(kg min)
λ_{G_up}	$\lambda_{VO_2}\alpha_3/\alpha_4$	mg/(kg min)
λ_{I_e}	$\lambda_{VO_2}\alpha_5/\alpha_6$	μU/ml
λ_{IL6}	$\lambda_{VO_2}\kappa_{\mathrm{SR}}/\kappa_{\mathrm{IL6}}$	pg/ml

Table B.2
Parameters used for the auxiliary functions building upon q_h (top) and the auxiliary functions building upon q_e (bottom). Standard values or the formula and the respective units are given in columns 2 and 3 [8,9].

Parameter	Definition	Unit
α_M	150	mg/dl
α_{ISR}	1.2	–
$\phi_{\max}$	4.55	1/day
α_P	41.77	μU/(μg day)
ζ_I	10^{-4}	–
κ_n	$10^6/\lambda_t$	(pg/ml) day
$\alpha_{\max}$	9	1/day
α_A	0.44	–
α_B	0.8	1/day
ζ_2	10^{-4}	–
$\gamma_{\max}$	0.2	–
γ_S	99.9	–
γ_n	1	–
γ_θ	0.1	–
$\kappa_{\sigma\mathrm{s}}$	75	mg/dl
$\sigma_{\mathrm{ISR}\max}$	600	μU/(μg day)
σ_{ISRs}	0.1	–
σ_{ISRn}	0.1	–
σ_{ISRk}	1	–
$\sigma_{\mathrm{M}\max}$	1	–
σ_{Ms}	0.2	–
σ_{Mn}	0.02	–
σ_{Mk}	0.2	–
σ_B	3	μU/(μg day)

The parameters related to the state variable VL are reported below together with the long-term state variables. The physical activity parameters ν and δ need to be chosen to allow for a maximum of 400 min of exercise per week, the intensity parameter ξ needs to lie within $[0, 92]$%.

A list of the parameters introduced for the auxiliary functions can be found in Table B.2.

All of these parameters are constrained to be positive.

A list of the parameters introduced for the long-term equations can be found in Table B.3.

Table B.3
Parameters related to the system of ODEs for $\mathbf{y_2}$ (top), the scaling of $\mathbf{y_2}$ (middle) and the initial conditions for $\mathbf{y_2}$ (bottom). Standard values or the formula and the respective units are given in columns 2 and 3 [8,9].

Parameter	Definition	Unit
κ_s	$-\log(0.8)/80640$	1/min
θ_{S_1}	0.18	ml/(μU day)
τ_{S_1}	150	day
ζ_3	1.4	–
k_{n,S_1}	$5\times10^6/\lambda_t$	(pg/ml) day
τ_Γ	2.14	day
τ_Σ	249.9	day
τ_B	8570	day
υ	5	litre
κ	700	1/day
ρ_0	864	mg/(dl day)
ω	70	kg
υ_g	117	dl
η_0	1.44	1/day
λ_{VL}/λ_t	$(\lambda_{IL6}/\kappa_s)/\lambda_t$	(pg/ml) day
λ_{S_1}	$S_{1,0}$	ml/(μU day)
λ_Γ	$\gamma_{\max}$	–
λ_B	B_0	mg
λ_I	I_0	μU/ml
λ_G	G_0	mg/dl
$\lambda_{I_e I}$	λ_{I_e}/λ_I	–
ρ_λ	ρ_0/λ_G	1/day
λ_{tG}	$\lambda_t/(\lambda_G\upsilon_g)$	min/(mg day)
$\lambda_{S_1 I}$	$\lambda_{S_1}\lambda_I$	1/day
VL_0	0	(pg/ml) min
$S_{1,0}$	0.8	ml/(μU day)
Γ_0	−0.00666	–
Σ_0	536.67	μU/ (μg day)
B_0	1000.423	mg
I_0	9.025	μU/ml
G_0	99.7604	mg/dl
$\Gamma_{0\lambda}$	Γ_0/λ_Γ	–
$\Sigma_{0\lambda}$	Σ_0/λ_Σ	–

The units of some parameters in Table B.3 are scaled with λ_t in order to be in days. Based on expert opinion, the initial conditions should be in the following intervals: $S_{1,0}\in[0,0.8]$, $\Gamma_0\in[-0.1,0.1]$, $\Sigma_0\in[3,600]$, $B_0\in[0,9000]$, $I_0\in[0,100]$, $G_0\in[0,600]$.

Appendix C. Model reduction

C.1. Analytical solution of the short-term equations

We calculate the analytical solution VO_2 from System (3) first in the interval $[0,\delta]$, where the control $u(t)=1$, then use the value at δ as initial condition to solve the ODEs analytically in the interval (δ,ν), where $u(t)=0$:

Lemma 1. *The solution to* $VO_2'(t)=\lambda_t\theta\big(1-VO_2(t)\big)$ *for* $0<t\le\delta$ *with initial condition* $VO_2(0)=0$ *is given by*

$$VO_2(t)=1-e^{-\lambda_t\theta t}.$$

Inserting δ yields $VO_2(\delta)=1-e^{-\lambda_t\theta\delta}$, which is the initial condition for the next interval:

Lemma 2. *The solution to* $VO_2'(t)=-\lambda_t\theta VO_2(t)$ *for* $\delta<t<\nu$ *with initial condition* $VO_2(\delta)=1-e^{-\lambda_t\theta\delta}$ *is given by*

$$VO_2(t)=\big(e^{\lambda_t\theta\delta}-1\big)e^{-\lambda_t\theta t}.$$

Calculating the analytical solution for the other four state variables from System (3) (G_{pr}, G_{up}, I_{e}, $IL6$) follows the same steps, additionally using the analytical solution of VO_2. For the sake of simplicity, we just illustrate it for G_{pr}:

Lemma 3. *The solution to* $G_{\mathrm{pr}}'(t)=\lambda_t\alpha_2\big(1-e^{-\lambda_t\theta t}-G_{\mathrm{pr}}(t)\big)$ *for* $0<t\le\delta$ *with initial condition* $G_{\mathrm{pr}}(0)=0$ *is given by*

$$G_{\mathrm{pr}}(t)=1+\frac{\alpha_2}{\theta-\alpha_2}e^{-\lambda_t\theta t}-\frac{\theta}{\theta-\alpha_2}e^{-\lambda_t\alpha_2 t}.$$

Inserting δ yields the initial condition for the next interval:

Lemma 4. *The solution to*

$$G_{\mathrm{pr}}'(t)=\lambda_t\alpha_2\Big(\big(e^{\lambda_t\theta\delta}-1\big)e^{-\lambda_t\theta t}-G_{\mathrm{pr}}(t)\Big)$$

for $\delta<t<\nu$ *with initial condition*

$$G_{\mathrm{pr}}(\delta)=1+\frac{\alpha_2}{\theta-\alpha_2}e^{-\lambda_t\theta\delta}-\frac{\theta}{\theta-\alpha_2}e^{-\lambda_t\alpha_2\delta}$$

is given by

$$G_{\mathrm{pr}}(t)=\frac{\theta}{\theta-\alpha_2}\big(e^{\lambda_t\alpha_2\delta}-1\big)e^{-\lambda_t\alpha_2 t}-\frac{\alpha_2}{\theta-\alpha_2}\big(e^{\lambda_t\theta\delta}-1\big)e^{-\lambda_t\theta t}.$$

C.2. Analytical average for the short-term equations

To calculate the average μ_{VO_2} of $VO_2(t)$ in the interval $[0,\nu)$, we start with

$$\int_0^\delta VO_2(t)\,\mathrm{d}t=\int_0^\delta 1-e^{-\lambda_t\theta t}\,\mathrm{d}t=\delta-\frac{1}{\lambda_t\theta}\big(1-e^{-\lambda_t\theta\delta}\big),$$

$$\begin{aligned}\int_\delta^\nu VO_2(t)\,\mathrm{d}t&=\frac{1}{\lambda_t\theta}\big(e^{\lambda_t\theta\delta}-1\big)\Big(e^{-\lambda_t\theta\delta}-e^{-\lambda_t\theta\nu}\Big)\\&=\frac{1}{\lambda_t\theta}\Big(1-e^{-\lambda_t\theta\delta}+e^{-\lambda_t\theta\nu}\big(1-e^{\lambda_t\theta\delta}\big)\Big).\end{aligned}$$

Combining these identities yields

$$\begin{aligned}\mu_{VO_2}&=\frac{1}{\nu}\int_0^\nu VO_2(t)\,\mathrm{d}t=\frac{1}{\nu}\left(\int_0^\delta VO_2(t)\,\mathrm{d}t+\int_\delta^\nu VO_2(t)\,\mathrm{d}t\right)\\&=\frac{1}{\nu}\left(\delta+\frac{1}{\lambda_t\theta}\Big(e^{-\lambda_t\theta\nu}\big(1-e^{\lambda_t\theta\delta}\big)\Big)\right).\end{aligned}$$

Note that the result is approximately equal to δ/ν, which is the average value of $u(t)$.
For G_{pr}, it holds that

$$\int_0^\delta G_{\mathrm{pr}}(t)\,\mathrm{d}t=\delta-\frac{\theta}{\lambda_t\alpha_2(\theta-\alpha_2)}\big(1-e^{-\lambda_t\alpha_2\delta}\big)+\frac{\alpha_2}{\lambda_t\theta(\theta-\alpha_2)}\big(1-e^{-\lambda_t\theta\delta}\big),$$

and

$$\begin{aligned}\int_\delta^\nu G_{\mathrm{pr}}(t)\,\mathrm{d}t=&\frac{\theta}{\lambda_t\alpha_2(\theta-\alpha_2)}\Big(1-e^{-\lambda_t\alpha_2\delta}+e^{-\lambda_t\alpha_2\nu}\big(1-e^{\lambda_t\alpha_2\delta}\big)\Big)\\&-\frac{\alpha_2}{\lambda_t\theta(\theta-\alpha_2)}\Big(1-e^{-\lambda_t\theta\delta}+e^{-\lambda_t\theta\nu}\big(1-e^{\lambda_t\theta\delta}\big)\Big).\end{aligned}$$

And hence,

$$\begin{aligned}\mu_{G_{\mathrm{pr}}}&=\frac{1}{\nu}\left(\int_0^\delta G_{\mathrm{pr}}(t)\,\mathrm{d}t+\int_\delta^\nu G_{\mathrm{pr}}(t)\,\mathrm{d}t\right)\\&=\frac{1}{\nu}\left(\delta+\frac{\theta}{\lambda_t\alpha_2(\theta-\alpha_2)}\Big(e^{-\lambda_t\alpha_2\nu}\big(1-e^{\lambda_t\alpha_2\delta}\big)\Big)\right.\\&\qquad\left.-\frac{\alpha_2}{\lambda_t\theta(\theta-\alpha_2)}\Big(e^{-\lambda_t\theta\nu}\big(1-e^{\lambda_t\theta\delta}\big)\Big)\right).\end{aligned}$$

The mean values for the state variables G_{up}, I_{e} and $IL6$ are calculated analogously to G_{pr}.

Appendix D. Simulations for the approximation error analysis

To quantify the numerical error resulting from model reduction, we varied six system parameters and three initial conditions, as summarized in Table D.1.

Each parameter configuration is denoted by Θ_i, where $i=1,\dots,19\,683$. Both systems are simulated for $t_{\mathrm{end}}=1824$ days (corresponding to 5 years) and the solutions are compared every 2 days, i.e.,

Table D.1
Parameters (top) and initial conditions (bottom) that are varied for the numerical evaluation of the approximation error, resulting in $3^9 = 19\,683$ simulations.

Parameter	Values
ν	2,4,6
δ	30/1440,45/1440,60/1440
ξ	20,40,60
θ_{S_I}	0.18,0.28,0.38
τ_{S_I}	90,210,330
ω	50,90,130
B_0	800,1000,1200
I_0	5,10,15
G_0	70,90,110

at $t_m := 2m$, where $m = 1, \dots, 912$. To quantify the approximation error, two measures are used. The maximal deviation between the two models over the entire time horizon under consideration,

$$E_i^{\text{basal}} := \max_{m=1,\dots,912} |\mathbf{y_2}(t_m, \mathbf{y_1}, \Theta_i) - \widehat{\mathbf{y}_2}(t_m, \boldsymbol{\mu}, \Theta_i)| \in \mathbb{R}^7,$$

and the point-wise error after 5 years,

$$E_i^{5\text{y}} := \left(\mathbf{y_2}(t_{\text{end}}, \mathbf{y_1}, \Theta_i) - \widehat{\mathbf{y}_2}(t_{\text{end}}, \boldsymbol{\mu}, \Theta_i)\right) \in \mathbb{R}^7.$$

References

[1] D.P. P.R. Group, Reduction in the incidence of type 2 diabetes with lifestyle intervention or metformin, N. Engl. J. Med. 346 (6) (2002) 393–403. https://doi.org/10.1056/NEJMoa012512

[2] F.C. Bull, S. Al-Ansari, S. Biddle, K. Borodulin, M.P. Buman, G. Cardon, C. Carty, J.P. Chaput, S. Chastin, R. Chou, P.C. Dempsey, L. DiPietro, U. Ekelund, J. Firth, C.M. Friedenreich, L. Garcia, M. Gichu, R. Jago, P.T. Katzmarzyk, E. Lambert, M. Leitzmann, K. Milton, F.B. Ortega, C. Ranasinghe, E. Stamatakis, A. Tiedemann, R.P. Troiano, H.P. Van Der Ploeg, V. Wari, J.F. Willumsen, World health organization 2020 guidelines on physical activity and sedentary behaviour, Br. J. Sports Med. 54 (24) (2020) 1451–1462. https://doi.org/10.1136/bjsports-2020-102955

[3] M.R. Rooney, M. Fang, K. Ogurtsova, B. Ozkan, J.B. Echouffo-Tcheugui, E.J. Boyko, D.J. Magliano, E. Selvin, Global prevalence of prediabetes, Diabetes Care 46 (7) (2023) 1388–1394. https://doi.org/10.2337/dc22-2376

[4] R.N. Bergman, L.S. Phillips, C. Cobelli, Physiologic evaluation of factors controlling glucose tolerance in man: measurement of insulin sensitivity and beta-cell glucose sensitivity from the response to intravenous glucose, J. Clin. Invest. 68 (6) (1981) 1456–1467. https://doi.org/10.1172/JCI110398

[5] A. Roy, R.S. Parker, Dynamic modeling of exercise effects on plasma glucose and insulin levels, J. Diabetes Sci. Technol. 1 (3) (2007) 338–347. https://doi.org/10.1177/193229680700100305

[6] B. Topp, K. Promislow, G. Devries, R.M. Miura, D.T. Finegood, A model of beta-cell mass, insulin, and glucose kinetics: pathways to diabetes, J. Theor. Biol. 206 (4) (2000) 605–619. https://doi.org/10.1006/jtbi.2000.2150

[7] J. Ha, L.S. Satin, A.S. Sherman, A mathematical model of the pathogenesis, prevention, and reversal of type 2 diabetes, Endocrinology 157 (2) (2016) 624–635. https://doi.org/10.1210/en.2015-1564

[8] P.F. De Paola, A. Paglialonga, P. Palumbo, K. Keshavjee, F. Dabbene, A. Borri, The long-term effects of physical activity on blood glucose regulation: a model to unravel diabetes progression, IEEE Control Syst. Lett. 7 (2023) 2916–2921. https://doi.org/10.1109/LCSYS.2023.3290774

[9] P.F. De Paola, A. Borri, F. Dabbene, K. Keshavjee, P. Palumbo, A. Paglialonga, Modeling the cumulative benefits of regular physical activity on type 2 diabetes progression, Comput. Biol. Med. 198 (2025) 111194. https://doi.org/10.1016/j.compbiomed.2025.111194

[10] R.N. Bergman, Minimal model: perspective from 2005, Horm. Res. Paediatr. 64 (2005) 8–15. https://doi.org/10.1159/000089312

[11] M.C. Palumbo, M. Morettini, P. Tieri, F. Diele, M. Sacchetti, F. Castiglione, Personalizing physical exercise in a computational model of fuel homeostasis, PLoS Comput. Biol. 14 (4) (2018) e1006073. https://doi.org/10.1371/journal.pcbi.1006073

[12] M.C. Palumbo, A.A. De Graaf, M. Morettini, P. Tieri, S. Krishnan, F. Castiglione, A computational model of the effects of macronutrients absorption and physical exercise on hormonal regulation and metabolic homeostasis, Comput. Biol. Med. 163 (2023) 107158. https://doi.org/10.1016/j.compbiomed.2023.107158

[13] L. Multerer, S. Toniolo, S. Mitrović, M.C. Palumbo, A. Ravoni, P. Tieri, M. Forgione, L. Azzimonti, A computationally efficient deep learning-based surrogate model of prediabetes progression, in: 2024 IEEE International Conference on Bioinformatics and Biomedicine (BIBM), IEEE, Lisbon, 2024, pp. 6951–6958. https://doi.org/10.1109/BIBM62325.2024.10822298

[14] A. De Gaetano, T.A. Hardy, B. Beck, E. Abu-Raddad, P. Palumbo, J. Bue-Valleskey, N. Pørksen, Mathematical models of diabetes progression, Am. J. Physiol.-Endocrinol. Metab. 295 (6) (2008) E1462–E1479. https://doi.org/10.1152/ajpendo.90444.2008

[15] A. De Gaetano, T.A. Hardy, A novel fast-slow model of diabetes progression: insights into mechanisms of response to the interventions in the diabetes prevention program, PLoS ONE 14 (10) (2019) e0222833. https://doi.org/10.1371/journal.pone.0222833

[16] N. Bakhvalov, G. Panasenko, Homogenisation: Averaging Processes in Periodic Media, 36 of *Mathematics and its Applications*, Springer Netherlands, Dordrecht, Dordrecht, 1989.

[17] D. Cioranescu, P. Donato, An Introduction to Homogenization, number 17 in Oxford lecture series in mathematics and its applications, Oxford University Press, Oxford, Oxford, 1999.

[18] J.A. Sanders, F. Verhulst, J. Murdock, Averaging Methods in Nonlinear Dynamical Systems, 59 of *Applied Mathematical Sciences*, Springer New York, New York, New York, 2007. https://doi.org/10.1007/978-0-387-48918-6

[19] G.A. Pavliotis, A.M. Stuart, Multiscale Methods: Averaging and Homogenization, number 53 in Texts in Applied Mathematics, Springer, New York, New York, 2008.

[20] G. Allaire, A brief introduction to homogenization and miscellaneous applications, ESAIM: Proc. 37 (2012) 1–49. https://doi.org/10.1051/proc/201237001

[21] S. Torquato, Random Heterogeneous Materials, 16 of *Interdisciplinary Applied Mathematics*, Springer New York, New York, New York, 2002. https://doi.org/10.1007/978-1-4757-6355-3

[22] U. Hornung (Ed.), Homogenization and Porous Media, 6 of *Interdisciplinary Applied Mathematics*, Springer New York, New York, New York, 1997. https://doi.org/10.1007/978-1-4612-1920-0

[23] F. Verhulst, Methods and Applications of Singular Perturbations, 50 of *Texts in Applied Mathematics*, Springer New York, New York, New York, 2005. https://doi.org/10.1007/0-387-28313-7

[24] H.P. Langtangen, G.K. Pedersen, Scaling of Differential Equations, Springer International Publishing, Cham, Cham, 2016. https://doi.org/10.1007/978-3-319-32726-6

[25] M. Morettini, M.C. Palumbo, M. Sacchetti, F. Castiglione, C. Mazzà, A system model of the effects of exercise on plasma interleukin-6 dynamics in healthy individuals: role of skeletal muscle and adipose tissue, PLoS ONE 12 (7) (2017) e0181224. https://doi.org/10.1371/journal.pone.0181224

[26] J. Li, Y. Kuang, C.C. Mason, Modeling the glucose-insulin regulatory system and ultradian insulin secretory oscillations with two explicit time delays, J. Theor. Biol. 242 (3) (2006) 722–735. https://doi.org/10.1016/j.jtbi.2006.04.002

[27] P.S. Shabestari, S. Panahi, B. Hatef, S. Jafari, J.C. Sprott, A new chaotic model for glucose-insulin regulatory system, Chaos, Solitons Fractals 112 (2018) 44–51. https://doi.org/10.1016/j.chaos.2018.04.029

[28] M. Lenatti, M. Zaffalon, A. Antonucci, P.F. De Paola, L. Multerer, M. Mongelli, A. Paglialonga, L. Azzimonti, Counterfactual inference using ordinary differential equations to assess the effect of physical activity on type 2 diabetes onset, in: Artificial Intelligence in Medicine, 15734, Springer Nature Switzerland, Cham, 2025, pp. 212–221. https://doi.org/10.1007/978-3-031-95838-0_21